Journal of Materials Chemistry A

Accepted Manuscript

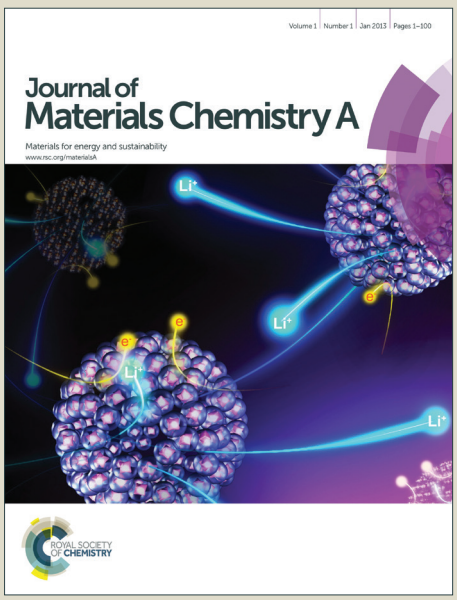

ROYAL SOCIETY OF CHEMISTRY

www.rsc.org/materialsA

Cite this: DOI: 10.1039/c0xx00000x

www.rsc.org/xxxxxx

ARTICLE TYPE

The Synthesis of Core-shell MnO_2/3D-Ordered Hollow Carbon Sphere Composite and Its Superior Electrochemical Capability for Lithium Ion Battery

Zang Jun‡, Chen Jia-jia‡, Zhang Cheng-long, Qian Hang, Zheng Ming-sen*,and Dong Quan-feng*

Received (in XXX, XXX) XthXXXXXXXXX 20XX, Accepted Xth XXXXXXXXX 20XX
DOI: 10.1039/b000000x

A hierarchical core-shell MnO_2/3D-ordered hollow carbon sphere composite was designed and synthesized by using the hollow carbon sphere (HCS) as carbon matrix. It exhibited an excellent cycling and high current density performance with a stable and reversible capacity of 420 mAh g^{-1} at 1 A g^{-1} (based on the whole mass of composite) as a potential anode material for high power lithium ion batteries. The excellent performance of MnO_2/HCS composite should owe to the synergistic effect of hierarchical architecture combined with nano-MnO_2 and porous structure of HCS.

Ongoing numerous research efforts are focused on searching for carbon alternatives in the hope of finding materials with both larger capacities and slightly more positive intercalation voltages compared to Li/Li^+, so as to minimize any risks of Li dendrite formation at the end of fast recharging, which are associated with safety problems. Such an effort resulted in the emergence of transition metal oxides (TMOs) which have been considered as the most promising anode materials in next-generation lithium ion batteries (LIBs).[1,2] Among the TMOs, manganese oxides have attracted great attention due to their various crystalline structures with different physical and electrochemical properties.[3–6] As an anode material, the theoretical capacity of MnO_2 with a moderate discharge potential (~0.4-0.5 V vs. Li/Li^+) would be high up to 1233 mAh g^{-1} (based on a 'conversion mechanism') which is almost the highest among all TMOs and more than 3 times larger compared with a commercial graphite anode (372 mAh g^{-1}).[7–9] Meanwhile, it is resource-abundant and environmental friendliness.[10] Actually, birnessite-type MnO_2 with high reversible capacity can be used as an anode electrode when the reversible conversion mechanism is enabled by the formation of nanometer-sized (<5 nm) Mn grains uniformly dispersed in a Li_2O matrix during the manganese oxide reduction reaction. [4,9] The nanometer-sized intact interface between Mn grains and Li_2O makes the reverse reaction kinetically favorable. Nevertheless, the developing of MnO_2 as an anode material for lithium ion batteries is still hindered by achieving a complete conversion reaction of MnO_2, the volume change and particles pulverization during lithiation/delithiation process.[4,11]

It has been pointed out that decreasing the particle size to nano-scale and combining with conductive matrix, such as carbon nanotubes and graphene nanosheets, are effective ways to improve the electrochemical performances of TMO anodes.[12–14] The conductive matrix would not only benefit to a shorter lithium ion transportation path and convenient electron transfer, but also accommodation of volume expansion during battery cycling. Nevertheless, previous investigation on MnO_2 as an anode material demonstrated only a partial conversion reaction of MnO_2/carbon nanotubes (CNTs) composite, with a reversible capacity of 801 mAh g^{-1} in the first 20 cycles at the current density of 100 mA g^{-1}. [4] Until now, it is still a challenge to fully release the capacity of MnO_2.

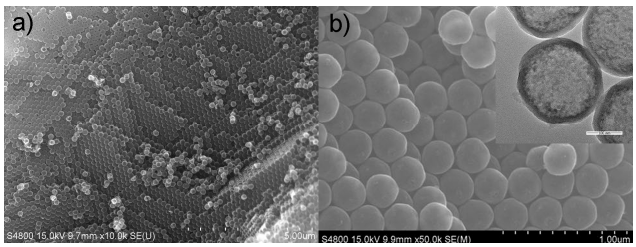

Fig. 1 SEM images a) and b) showing the morphologies of 3D ordered HCS, the inset picture in b) is the TEM image of 3D ordered HCS.

Herein, we firstly report an almost complete and highly reversible conversion reaction of MnO_2 with a 4e process by utilizing 3D ordered hollow carbon spheres (HCS) as conductive matrix. 3D ordered HCS is usually considered as an excellent conductive framework due to its spherality, porosity and high specific surface area.[15,16] By using PMMA emulsion as the template and resorcinol-formaldehyde as the carbon precursor, the template was decomposed and then the precursor was carbonized into uniform structure of HCS after sintering at 800 ℃ for 1 h under N_2 atmosphere. As shown in Fig. 1a and b, all hollow carbon spheres, forming a close packed structure, are uniform in size with an average diameter of ~220 nm. The HRTEM micrograph (the inset picture of Fig. 1b) reveals that the carbon sphere shell is in a uniform thickness around 20 nm. The external surface of HCS is very smooth and clean, indicating no impurities were left over the carbonization process. The HCS exhibits a Type IV isotherm with a Brunauer-Emmett-Teller (BET) surface area of 922.56 m^2 g^{-1} and a mono-mesoporous size of around 4 nm, derived

from the N_2 porosimetry using the Barrett-Joyner-Halenda (BJH) method (see Fig. S1, ESI).[17]

Nano-structured MnO_2 was in-situ grown on the surface of HCS by a facile redox method, using P123 as a surfactant. $KMnO_4$ was reduced by the external carbon layer of HCS and then nano-crystalline MnO_2 is uniformly grown in-situ on the 3D ordered HCS surfaces, following the reaction process: 4 MnO_4^- + 3 C + H_2O → 4 MnO_2 + CO_3^{2-} + 2 HCO_3^-.[18] Composites with different MnO_2 ratio were obtained by adjusting the molar ratio of $KMnO_4$ and HCS, determined by TG/DTA under a dry air atmosphere at a heating rate of 5° min^{-1}. The mass loading of MnO_2 is calculated to be 68%, 47% and 35%, respectively (see Fig. S2, ESI). XRD patterns of the HCS and MnO_2/HCS composites with different MnO_2 loadings are shown in Fig. S3 (ESI). The XRD peaks at 2θ=12°, 37° and 66° can be readily indexed to the (001), (111) and (020) planes of birnessite-type MnO_2.[4] With the increasing of molar of $KMnO_4$, the reduction extent of HCS was increasing gradually and then the hierarchical structures of MnO_2/HCS composites were damaged severely (Fig. 2a-d). For a low molar ratio of $KMnO_4$/HCS, MnO_2 could be uniformly grown on the surface of HCS. When $KMnO_4$ was excess, HCS in the composite was almost disappeared (Fig. 2d). This indicates that only in a reasonable molar ratio of $KMnO_4$/HCS, a uniform morphology and stable structure of MnO_2/HCS composite can be obtained. As shown in Fig. 2b, core-shell structure of MnO_2/HCS-47% composite forms an interwoven 3D network structure with a size of ~100 nm in length and ~5 nm in width. The Mn and C element mappings (Fig. 2e-g) further confirm that nano-structure MnO_2 has an intact contact with the surface of HCS without significant fraction. The SAED pattern (see Fig. S4, ESI) also clearly demonstrated that the as-prepared MnO_2 was nano-polycrystalline which was in agreement with the result of the broadened XRD peaks of MnO_2/HCS composites.

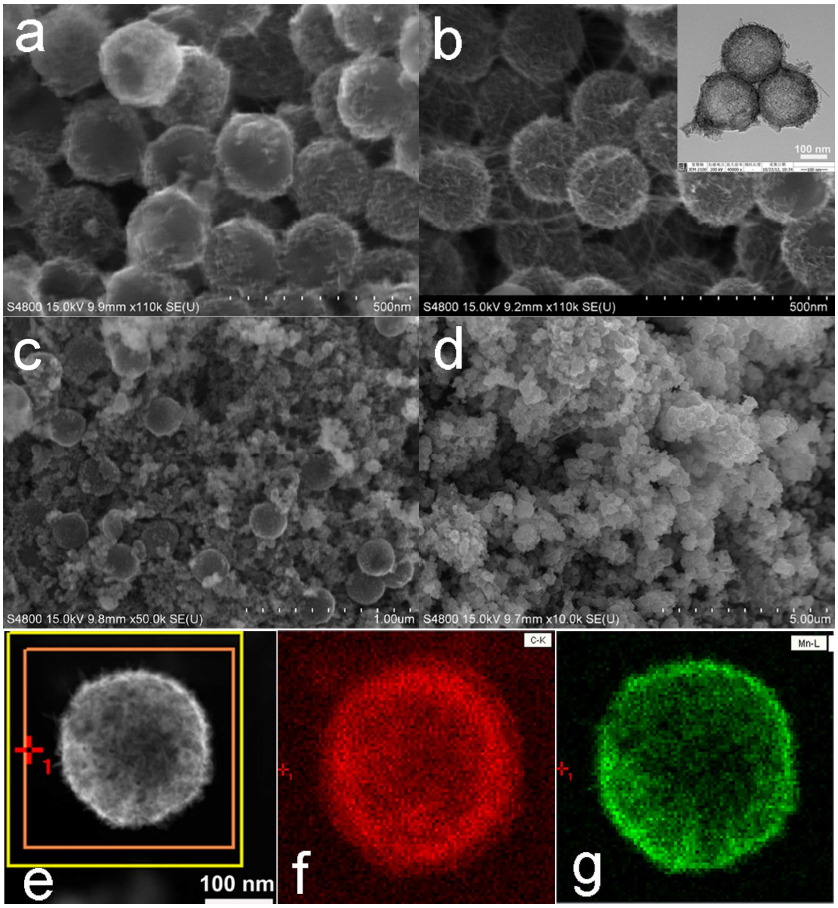

Fig. 2 The SEM images showing the different morphologies of MnO_2/HCS composites prepared by adjusting the molar ratio of $KMnO_4$/HCS: a) MnO_2/HCS-35% ; b) MnO_2/HCS-47%; c) MnO_2/HCS-68% and d) pure MnO_2; the inset picture in b) is the TEM image of MnO_2/HCS-47; e-g) STEM image and corresponding C and Mn elemental mappings of MnO_2/HCS-47%.

When tested as anode materials for lithium ion batteries, the electrochemical performances of the MnO_2/HCS composites were greatly influenced by their morphologies and hierarchical structures. As a conductive carbon matrix, HCS also exhibits superior rate and cyclic capability. No obvious fading of the discharge capacity is observed during 100 cycles after activation for the first 3 cycles under a current density of 0.1 A g^{-1} (Fig. 3a). In addition, it could reserve a stable capacity of 116.7 mAh g^{-1} at 10 A g^{-1} and has the ability to regain almost 324.5 mAh g^{-1} when the current density returns to 0.1 A g^{-1} (see Fig. S5, ESI).

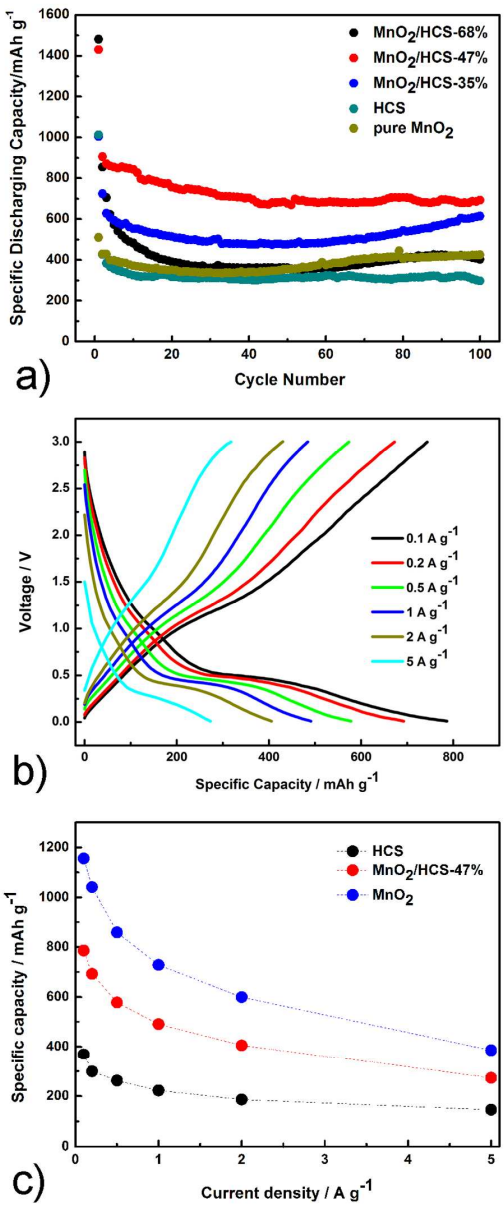

Fig. 3 a) The cycle performances of different mass loading of MnO_2/HCS composites; b) the charging-discharging curves of MnO_2/HCS-47% at different current densities; c) the comparative rate performances of HCS, MnO_2/HCS-47% composite and the capacities based on MnO_2 subtracting the capacity contribution of HCS from MnO_2/HCS-47% composite.

Inspired by the stable electrochemical performance of HCS during lithiation/delithiation process, nano-MnO_2 is in-situ grown on ordered HCS surfaces, aiming at building novel composites with expected electrochemical properties. As shown in Fig. 3a, most of the MnO_2/HCS composites experience a marked fading in capacity during the initial cycles, which has been ascribed to the lithium ion consumption in the decomposition of the electrolyte and formation of solid electrolyte interface (SEI) film. MnO_2/HCS-47% composite exhibits the best electrochemical performance among all the as-prepared products. It retains a stable capacity at 692.5 mAh g^{-1} (based on the whole mass of MnO_2/HCS composite) during 100 cycles at 0.1 A g^{-1} which is about 81% in comparison with the initial reversible capacity. MnO_2/HCS-35% shows a stable cycle performance but with a low specific capacity due to its low MnO_2 loading while pure MnO_2 and MnO_2/HCS-68% deliver low capacities and suffer capacities degrading during cycling which are caused by the high active material mass loading and destroyed structure of HCS.

Meanwhile, the comparative studies of the voltage versus capacity profiles at different rates (Fig. 3b) show that MnO_2/HCS-47% suffers a high rate discharging-charging testing with only small polarization. It could represent the typical electrochemical behavior whilst deliver a reversible capacity of 420 mAh g^{-1} based on the whole mass of composite at the current density of 1 A g^{-1}, which is still more than the theoretical capacity of graphite (372 mAh g^{-1}). Even increasing current density up to 5 A g^{-1}, it could also deliver a specific capacity of 180 mAh g^{-1}. If the capacity contribution of HCS is subtracted from MnO_2/HCS composite at the same current density (Fig. 3c, Fig. S5 and S6, ESI), MnO_2 could achieve a reversible stable capacity of 1107.5 mAh g^{-1} at 0.1 A g^{-1} within 100 cycles which is close to its theoretical of 1233 mAh g^{-1}, indicating that an almost complete conversion reaction of MnO_2 is achieved within lithiation/delithiation process. Nevertheless, rate performances of other MnO_2/HCS composites could not exhibit such stable or high capacity retention during cycling (see Table S1, Fig. S7, ESI).

If the electrochemical reaction between MnO_2 and Li can be described as a reversible 'conversion mechanism', the formation of Mn/Li_2O should lead to a theoretical capacity of 1233 mAh g^{-1}. It is commonly believed that Li ion transport could be enhanced by the nano-structure while electron mobility is highly dependent on the interface of conductive matrix.[19] Therefore, the superior electrochemical performance of MnO_2/HCS-47% composite should be attributed to the synergistic effect of hierarchical architecture. As illustrated in Fig. 4a, the high porosity of HCS facilitates the penetration of electrolyte into nanopores while the high specific surface area can be in favor of increasing the electron transfer within its sphere structure. Meanwhile, HCS shows excellent structure stability during the Li^+ intercalation/deintercalation process, even suffering from a very high current density. After in-situ growing of MnO_2 on the ordered HCS surfaces, the Li^+ diffusion and electron transfer at the interface of nano-scale MnO_2 and HCS can be improved greatly. As confirmed by the EIS (Fig. 4b), HCS has the lowest charge transfer resistance (Rct) and the Rct of the MnO_2/HCS composites increases when the mass loading of MnO_2 increases. Meanwhile, XPS result (Fig. 4d) shows the Mn 2p spectrum, the peaks of Mn 2p3/2 and 2p1/2 which are centered at 642.3 and 654.1 eV, respectively, with a spin-energy separation of 11.8 eV, are in good agreement with reported data.[3,20] At the end of first discharging of MnO_2/HCS-47%, XPS peaks of Li 1s centered at 54.7 eV confirms the formation of Li_2O. And the binding energies of Mn 2p3/2 and 2p1/2 decrease due to the reduction of MnO_2 to metallic Mn (Fig. 4e and f).[3,21] According to the results of XPS spectrum, MnO_2 can be reduced into Mn and Li_2O in the initial lithiation process. Considering the highly reversible charging-discharging capacities of 1107.5 mAh g^{-1},

an almost complete conversion reaction of MnO_2 can be achieved in MnO_2/HCS-47%. This advantage of synergistic effect of hierarchical architecture can be further confirmed by the extremely long cycle performance under a high current density (Fig. 4c). There is no obvious capacity fading during 500 cycles and retains a stable 420 mAh g^{-1} specific reversible capacity when tested at 1 A g^{-1}. This excellent electrochemical reversibility and structural stability should ascribe to the unique hierarchical structure by withstanding the huge volume changes during charging/discharging process.

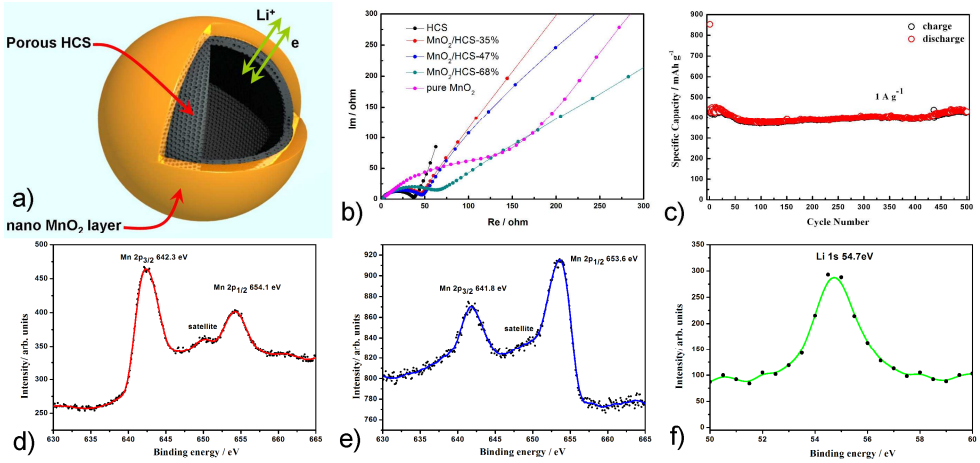

Fig. 4 a) Illustration of the synergistic effect of hierarchical architecture of core-shell MnO_2/HCS composite; b) Comparative AC impedance studies of HCS, pure MnO_2 and different MnO_2 mass loading MnO_2/HCS composites; c) Long cycling and high rate testing of MnO_2/HCS-47% at 1 A g^{-1}, specific capacities were calculated based on the whole mass of MnO_2/HCS-47% composite; and XPS spectra of Mn element in MnO_2/HCS-47% composite before (d) and after (e) first discharge process. Formation of Li_2O (f) during the initial lithiation process has been confirmed using XPS.

Conclusions

In summary, we have prepared MnO_2/HCS composite with hierarchical hollow structure. A thin layer of poor crystallized birnessite-type MnO_2 can be homogenously in-situ grown on the external surface of HCS. The superior electrochemical performances should be attributed to the synergistic effect of hierarchical architecture. First, the conductive HCS matrix improves the ion and electron transportation in MnO_2 bulk phase while also decreases the resistance at the interface of electrode/electrolyte. Secondly, the intact contact of nano MnO_2 with the surface of HCS provides good elasticity retention to retard the volume change during Li^+ insertion/extraction of MnO_2 bulk phase, thus facilitating the repetitive cycling. Last but not least, such unique structure of hollow core-shell MnO_2/carbon composites will probably have potential applications in electrochemical power source, sensors and other fields, such as the catalyst for lithium air battery.

We gratefully acknowledge the financial support from the Key Project of NSFC (U1305246, 21321062), the Major Project funded by Xiamen city (3502Z20121002).

Notes and references

State Key Laboratory of Physical Chemistry of Solid Surfaces, Department of Chemistry, College of Chemistry and Chemical Engineering, XiamenUniversity, Xiamen, Fujian, 361005, China
Fax: +86-592-2185905; Tel: +86-592-2185905;
**Corresponding author e-mail: gfdong@xmu.edu.cn and mszheng@xmu.edu.cn.*

†Electronic Supplementary Information (ESI) available: Detailed experimental procedures. XRD、TGA、Rate performance and discharge-charge curves. See DOI: 10.1039/b000000x/

‡ These two authors, Jun Zang and Jia Jia Chen, contributed equally to this work.

1. P. Poizot, S. Laruelle, S. Grugeon, L. Dupont, and J.-M. Tarascon, *Nature*, 2000, **407**, 496.
2. P. L. Taberna, S. Mitra, P. Poizot, P. Simon, and J. M. Tarascon, *Nat Mater*, 2006, **5**, 567.
3. V. B. R. Boppana and F. Jiao, *Chem. Commun.*, 2011, **47**, 8973.
4. F. Y. Cheng, J. Chen, X. L. Gou, and P. W. Shen, *Adv. Mater.*, 2005, **17**,2753.
5. S. Chen, J. Zhu, X. Wu, Q. Han, and X. Wang, *ACS Nano*, 2010, **4**, 2822.
6. M. Kundu, C. C. A. Ng, D. Y. Petrovykh, and L. Liu, *Chem. Commun.*, 2013, **49**, 8459.
7. A. L. M. Reddy, M. M. Shaijumon, S. R. Gowda, and P. M. Ajayan, *Nano Lett.*, 2009, **9**, 1002.
8. C. X. Guo, M. Wang, T. Chen, X. W. Lou, and C. M. Li, *Adv. Energy Mater.*, 2011, **1**, 736.
9. Y. Wang, Z. J. Han, S. F. Yu, R. R. Song, H. H. Song, K. (Ken) Ostrikov, and H. Y. Yang, *Carbon*, 2013, **64**, 230.
10. J. Zhao, Z. Tao, J. Liang, and J. Chen, *Cryst. Growth Des.*, 2008, **8**, 2799.
11. M. S. Wu and P. C. Chiang, *J. Phys. Chem. B*, 2005, **109**, 23279.
12. M. V. Reddy, T. Yu, C. H. Sow, Z. X. Shen, C. T. Lim, G. V. Subba Rao, and B. V. R. Chowdari, *Adv. Funct. Mater.*, 2007, **17**, 2792.
13. L. Shen, H. Li, E. Uchaker, X. Zhang, and G. Cao, *Nano Lett.*, 2012, **12**, 5673.
14. L. Li, A.-R. O. Raji, and J. M. Tour, *Adv. Mater.*, 2013, **25**, 6298
15. Y. Li, T. Li, M. Yao, and S. Liu, *J. Mater. Chem.*, 2012, **22**, 10911.
16. F. Böttger-Hiller, P. Kempe, G. Cox, A. Panchenko, N. Janssen, A. Petzold, T. Thurn-Albrecht, L. Borchardt, M. Rose, S. Kaskel, C. Georgi, H. Lang, and S. Spange, *Angew. Chem. Int. Ed.*, 2013, **52**, 6088.
17. A. Lu, A. Kiefer, W. Schmidt, and F. Schüth, *Chem. Mater.*, 2004, **16**, 100.
18. Z. Lei, J. Zhang, and X. S. Zhao, *J. Mater. Chem.*, 2011, **22**, 153.
19. D. Wang, D. Choi, J. Li, Z. Yang, Z. Nie, R. Kou, D. Hu, C. Wang, L. V. Saraf, J. Zhang, I. A. Aksay, and J. Liu, *ACS Nano*, 2009, **3**, 907.
20. D. Liu, Q. Zhang, P. Xiao, B. B. Garcia, Q. Guo, R. Champion, and G. Cao, *Chem. Mater.*, 2008, **20**, 1376.
21. M. C. Biesinger, B. P. Payne, A. P. Grosvenor, L. W. M. Lau, A. R. Gerson, and R. S. C. Smart, *Appl. Surf. Sci.*, 2011, **257**, 2717.